Neuron
Article

Secreted Semaphorins from Degenerating Larval ORN Axons Direct Adult Projection Neuron Dendrite Targeting

Lora B. Sweeney,[1,2,3,6] Ya-Hui Chou,[1,2,7,10] Zhuhao Wu,[1,5,10] William Joo,[1,2,3,10] Takaki Komiyama,[1,2,3,8] Christopher J. Potter,[1,2,9] Alex L. Kolodkin,[1,5] K. Christopher Garcia,[1,4] and Liqun Luo[1,2,3,*]
[1]Howard Hughes Medical Institute
[2]Department of Biology
[3]Neurosciences Program
[4]Department of Molecular and Cellular Physiology
Stanford University, Stanford, CA 94305, USA
[5]The Solomon H. Snyder Department of Neuroscience, Johns Hopkins University School of Medicine, Baltimore, MD 21205, USA
[6]Present address: The Salk Institute for Biological Studies, La Jolla, CA 92037, USA
[7]Present address: Institute of Cellular and Organismic Biology, Academia Sinica, Taipei 11529 Taiwan
[8]Present address: Neurobiology Section, Department of Neurosciences and Center for Neural Circuits and Behavior, University of California, San Diego, CA 90293, USA
[9]Present address: The Solomon H. Snyder Department of Neuroscience, Johns Hopkins University School of Medicine, Baltimore, MD 21205, USA
[10]These authors contributed equally to this work
*Correspondence: lluo@stanford.edu
DOI 10.1016/j.neuron.2011.09.026

SUMMARY

During assembly of the *Drosophila* olfactory circuit, projection neuron (PN) dendrites prepattern the developing antennal lobe before the arrival of axons from their presynaptic partners, the adult olfactory receptor neurons (ORNs). We previously found that levels of transmembrane Semaphorin-1a, which acts as a receptor, instruct PN dendrite targeting along the dorsolateral-ventromedial axis. Here we show that two secreted semaphorins, Sema-2a and Sema-2b, provide spatial cues for PN dendrite targeting. Sema-2a and Sema-2b proteins are distributed in gradients opposing the Sema-1a protein gradient, and Sema-1a binds to Sema-2a-expressing cells. In Sema-2a and Sema-2b double mutants, PN dendrites that normally target dorsolaterally in the antennal lobe mistarget ventromedially, phenocopying cell-autonomous Sema-1a removal from these PNs. Cell ablation, cell-specific knockdown, and rescue experiments indicate that secreted semaphorins from degenerating larval ORN axons direct dendrite targeting. Thus, a degenerating brain structure instructs the wiring of a developing circuit through the repulsive action of secreted semaphorins.

INTRODUCTION

The fly olfactory circuit provides an excellent system to study the developmental mechanisms that establish wiring specificity. In the adult olfactory system, each of the 50 classes of olfactory receptor neurons (ORNs) expresses a specific odorant receptor and targets its axons to a single glomerulus in the antennal lobe. Each class of projection neurons (PNs) sends its dendrites to one of these 50 glomeruli to form synaptic connections with a particular ORN class. This precise connectivity allows olfactory information to be delivered to specific areas of the brain, thus enabling odor-mediated behaviors.

The assembly of the adult antennal lobe circuitry occurs during the first half of pupal development. At the onset of puparium formation, PN dendrites begin to generate a nascent neuropil structure that will develop into the adult antennal lobe. By 18 hr after puparium formation (APF), dendrites of a given PN class occupy a specific part of the antennal lobe which roughly corresponds to adult glomerular position, thus "prepatterning" the antennal lobe (Jefferis et al., 2004). Adult ORN axons invade the developing antennal lobe after 18 hr APF, and the one-to-one connectivity between ORN and PN classes is complete by 48 hr APF, when individual glomeruli emerge. This developmental sequence divides olfactory circuit wiring into two phases: an early phase (0–18 hr APF) when PN dendrites target independently of adult ORN axons, and a late phase (18–48 hr APF) when ORN axons and PN dendrites interact with each other to form discrete glomeruli (Luo and Flanagan, 2007). This study focuses on the early phase of PN dendrite targeting.

PNs are prespecified by their lineage and birth order to target dendrites to specific glomeruli (Jefferis et al., 2001). Transcription factors that distinguish between lineages and birth orders within lineages have begun to be identified (Komiyama et al., 2003; Zhu et al., 2006). These transcriptional programs presumably regulate differential expression of cell surface proteins in different classes of PNs to instruct their specific targeting within a common environment. So far, two kinds of instructive cell surface proteins have been identified. Semaphorin-1a

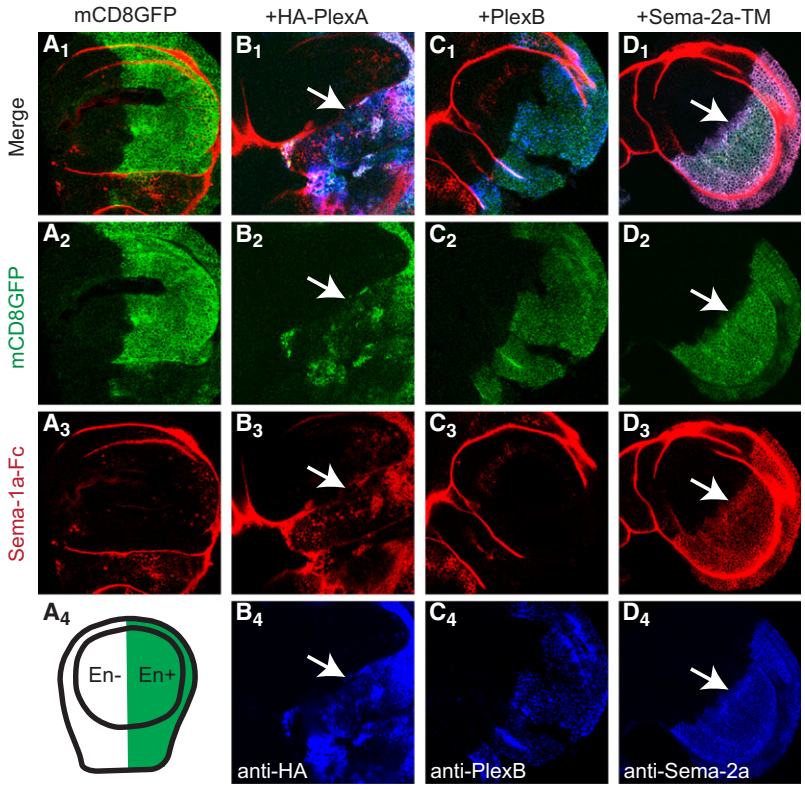

Figure 1. Sema-1a Binds Sema-2a-Expressing Cells

engrailed (*en*)-*GAL4* was used to drive, in the posterior compartment of the wing disc (A_4), *UAS-mCD8-GFP* alone (A), or *UAS-mCD8-GFP* together one of the following additional transgenes: *UAS-HA-PlexA* (B), *UAS-PlexB* (C), or *UAS-Sema-2a-TM* (D). Row 1 shows the merge of staining in rows 2–4; row 2 shows GFP fluorescence in the en^+ compartment; row 3 shows binding of Sema-1a-Fc in live wing discs followed by fixing and staining against Fc; row 4 shows antibody staining of overexpressed PlexA-HA, PlexB, and Sema-2a-TM. Sema-1a-Fc binds specifically to PlexA-HA- and Sema-2a-TM-expressing wing disc cells (arrows in B_3 and D_3). Note that Sema-1a-Fc was trapped nonspecifically in the wing disc folds of all samples during live staining. In addition, PlexA-HA overexpression disrupted wing disc compartment morphology. See Figure S1 for Sema-1a-Fc binding to neurons expressing Sema domain containing- proteins.

(Sema-1a), a transmembrane semaphorin, acts cell-autonomously as a receptor in PNs to direct the coarse targeting of their dendrites along the dorsolateral-ventromedial axis. PNs expressing high or low Sema-1a project to the dorsolateral or ventromedial antennal lobe, respectively, forming a protein gradient among PN dendrites (Komiyama et al., 2007). Capricious (Caps), a leucine-rich repeat domain-containing cell surface protein, is expressed in a subset of PNs. $Caps^+$ PNs and $Caps^-$ PNs target dendrites to glomeruli that form a "salt and pepper" pattern, and Caps appears to act as a binary determinant to ensure the segregation of $Caps^+$ and $Caps^-$ PN dendrites into distinct glomeruli (Hong et al., 2009). Combinations of global targeting mechanisms exemplified by Sema-1a and local binary choices exemplified by Caps may direct dendrite targeting of diverse PN classes.

What is the origin of PN wiring specificity in this circuit? We previously hypothesized that Sema-1a acts as a dendrite targeting receptor and responds to either a dorsolateral attractive cue or a ventromedial repulsive cue. In this way, PNs expressing different levels of Sema-1a are directed to distinct positions along the dorsolateral-ventromedial axis (Komiyama et al., 2007). Here we provide evidence that two secreted semaphorins, Sema-2a and Sema-2b, serve as key spatial cues. Interestingly, Sema-2a and Sema-2b produced by two distinct sources, larval ORNs and adult PNs, are responsible for PN dendrite targeting to dorsolateral and ventromedial glomeruli in the antennal lobe, respectively. The first case provides an interesting example of how a degenerating brain structure can instruct the wiring of a developing circuit.

RESULTS

Sema-1a Binds Sema-2a-Expressing Cells

Plexins and neuropilins are well known receptors for semaphorins when semaphorins act as ligands (Tran et al., 2007). Flies have two plexins, plexinA (PlexA) and plexinB (PlexB), but no neuropilins. Because plexins and semaphorins both contain Sema domains that act as the interface for their binding (Janssen et al., 2010; Liu et al., 2010; Nogi et al., 2010), we hypothesized that the ligand for Sema-1a likewise contains a Sema domain. To test whether Sema-1a binds to any of the Sema-domain containing proteins in the fly, we used the GAL4/UAS system (Brand and Perrimon, 1993) to express available Sema domain-containing UAS transgenes in ectopic cells. We then used Sema-1a-Fc (the Sema-1a extracellular domain fused to the human immunoglobulin Fc domain) as an affinity probe to test for Sema-1a binding to cells ectopically expressing a given Sema-domain-containing protein.

Engrailed-GAL4 (*en-GAL4*) drives UAS-transgene expression in the posterior compartment of the wing imaginal disc, with the anterior compartment serving as a negative control (Figure 1A_4). We performed binding experiments by incubating Sema-1a-Fc with live larval wing discs, followed by fixation and permeabilization to stain for Sema-1a-Fc and *en-GAL4*-overexpressed proteins. In wing discs expressing only the mCD8-GFP marker, Sema-1a-Fc did not exhibit any specific binding (Figure 1A). Wing disc cells expressing PlexA-HA exhibited strong Sema-1a-Fc binding (Figure 1B; PlexA overexpression also severely disrupted wing disc morphology). In contrast, Sema-1a-Fc did not bind to wing disc cells expressing PlexB (Figure 1C). These data are consistent with previous experiments demonstrating that PlexA, but not PlexB, binds to Sema-1a (Ayoob et al., 2006; Winberg et al., 1998b). Interestingly, Sema-1a-Fc also binds to wing disc cells expressing membrane-tethered Sema-2a (Sema-2a-TM; Figure 1D). This experiment suggests that Sema-2a could be a binding partner of Sema-1a.

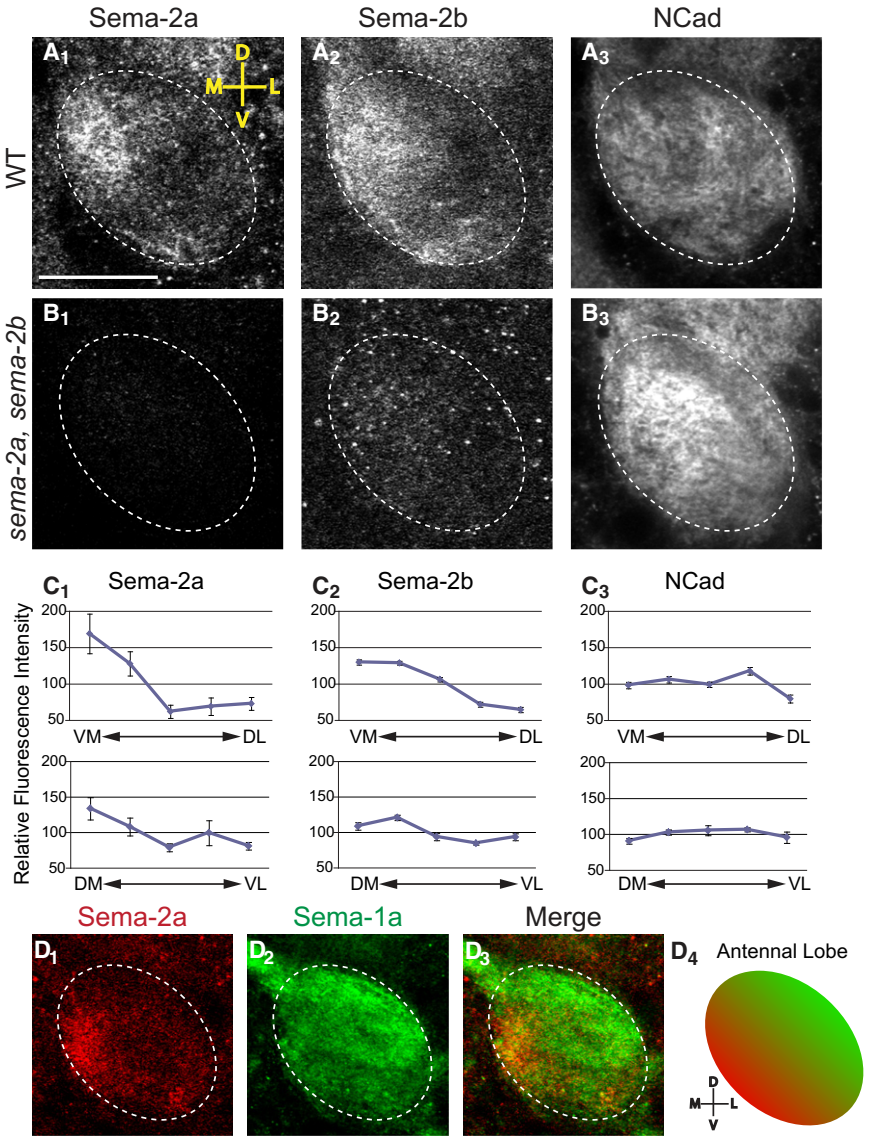

Figure 2. Sema-2a and -2b Are Enriched in the Ventromedial Antennal Lobe During PN Targeting

(A) At 16 hr APF, Sema-2a (A_1) and Sema-2b (A_2) are concentrated in the same ventromedial region of the WT antennal lobe (dotted oval). For comparison, the pan-neuropil N-cadherin (A_3) is more broadly distributed in the antennal lobe.

(B) At 16 hr APF, no detectable Sema-2a (B_1) or Sema-2b (B_2) staining in the *sema-2a sema-2b* double mutant antennal lobe, while N-cadherin is maintained (B_3).

(C) Relative fluorescence intensity quantified along the ventromedial-dorsolateral (VM-DL, top) and dorsomedial-ventrolateral (DM-VL, bottom) axis of the WT antennal lobe of Sema-2a (C_1), Sema-2b (C_2), and N-cadherin (C_3). See Experimental Procedures for description of the quantification procedure.

(D) At 16 hr APF, Sema-2a and Sema-1a show opposing expression patterns in the same brain. As previously shown in Komiyama et al. (2007), Sema-1a is high dorsolaterally. (D_4) Schematic summary. Green, Sema-1a. Red, Sema-2a. Scale bar represents 20 μm. Single 1 μm-confocal sections are shown for each panel.

Images from different paenls with (A), (B), and (D) came from the same antennal lobes. D, dorsal; V, ventral; M, medial; L, lateral. Figure S2 shows Sema-2a and Sema-2b distribution at earlier developmental stages.

We also performed binding experiments by incubating Sema-1a-Fc with live 24 hr APF pupal brains in which *OK107-GAL4* drives UAS transgene expression in mushroom body neurons and in neurons near the dorsal midline (see Figure S1A4 available online). Consistent with the results in wing disc, Sema-1a-Fc bound to PlexA (Figure S1B) but not PlexB (Figure S1C) expressing neurons. It also bound to membrane-tethered Sema-2a in midline neurons (Figure S1E). Moreover, Sema-1a-Fc consistently bound to overexpressed Sema-2a in its native, secreted form in the mushroom body neuropil (arrows in Figure S1D3), likely because neuropil retarded secreted Sema-2a diffusion and permitted recognition by Sema-1a-Fc. This raised the possibility that Sema-2a may be a binding partner of Sema-1a. However, we could not detect Sema-1a-Fc binding to *Drosophila* S2 cells expressing membrane tethered Sema-2a (data not shown), suggesting that Sema-1a-Fc binding to Sema-2a-expressing wing disc cells or neurons may be indirect (see Discussion). Nevertheless, the specific binding of Sema-1a-Fc to Sema-2a-expressing neurons prompted us to examine the role of Sema-2a and its close homolog Sema-2b in wiring of the olfactory circuit.

Sema-2a and Sema-2b Are Enriched in the Ventromedial Antennal Lobe Opposing Dorsolateral Sema-1a

Between 0 and 18 hr APF, PN dendrites extend into the antennal lobe, elaborate in the vicinity of their final glomerular target, and coalesce onto a small area that will eventually develop into a single glomerulus. Importantly, pioneering ORN axons do not reach the edge of the antennal lobe until 18 hr APF, and therefore much of the initial PN dendrite targeting is independent of adult ORNs (Jefferis et al., 2004). To examine the Sema-2a expression pattern during this early targeting phase, we used a monoclonal antibody against a C-terminal Sema-2a peptide (Winberg et al., 1998a). We also examined the expression pattern of Sema-2b, a highly-related semaphorin with 70% amino acid identity (84% similarity) to Sema-2a, using a polyclonal antibody against the entire Sema-2b protein (see Experimental Procedures).

At 16 hr APF, just prior to the arrival of adult ORN axons, Sema-2a and Sema-2b were highly enriched medially and ventromedially within the antennal lobe (Figures 2A_1 and 2A_2). Sema-2a and Sema-2b showed similar distribution patterns, although there was a subtle difference upon quantification: the

Sema-2a gradient was steeper in the ventromedial antennal lobe whereas that of Sema-2b was more gradual and extended further into the dorsolateral antennal lobe (Figure 2C). By comparison, the pan-neuropil marker N-cadherin was broadly distributed across the entire antennal lobe (Figure 2A$_3$), as were the distributions of all three proteins when quantified along the orthogonal dorsomedial-ventrolateral axis (Figure 2C). In *sema-2a sema-2b* homozygous double mutant flies (see below) at 16 hr APF, Sema-2a and Sema-2b staining in the antennal lobe was undetectable (Figure 2B), confirming both the specificity of the Sema-2 antibodies and the absence of protein in these mutants. In addition, these antibodies did not cross react, as *sema-2a* or *sema-2b* single mutants only lacked Sema-2a or -2b antibody staining, respectively (data not shown). We also examined expression of Sema-2a and Sema-2b at 0 hr, 6 hr, and 12 hr APF and found that their distribution patterns during these earlier time points were similar to those described above for 16 hr APF (Figure S2). These expression studies suggest that Sema-2a and Sema-2b can be used as cues for PN dendrite targeting along the dorsolateral-ventromedial axis.

At 16 hr APF, the ventromedial enrichment of Sema-2a/2b is in opposition to the previously shown dorsolateral-high Sema-1a gradient (Komiyama et al., 2007). Where Sema-2a was high, Sema-1a was low; where Sema-1a was high, Sema-2a was low (Figure 2D). These opposing expression patterns, in addition to our binding data, suggested that Sema-1a and Sema-2a/2b may function together during PN dendrite targeting to segregate PN dendrites along this axis. The onset of localized Sema-2a and Sema-2b expression (Figure S2) preceded that of Sema-1a (~6–12 hr APF) (Komiyama et al., 2007), consistent with a hypothesis that Sema-2a and Sema-2b instruct Sema-1a mediated PN dendrite targeting to the dorsolateral antennal lobe.

Sema-2a and Sema-2b Function Redundantly to Direct Dorsolateral-Targeting PN Dendrites

To test the requirement for secreted Sema-2a and Sema-2b in PN dendrite targeting, we utilized two P-element insertions at the *sema-2a* locus (Kolodkin et al., 1993) and a *piggyBac* insertion into *sema-2b* (Thibault et al., 2004). All mutations resulted in a complete loss of corresponding proteins during PN dendrite targeting as assessed by antibody staining (Figures 2B and S2). Because Sema-2a/2b are secreted proteins and thus likely function cell nonautonomously, we labeled individual or small groups of PNs in whole animal homozygous mutant flies. Flies homozygous for *sema-2b* were viable. A small fraction of flies homozygous for *sema-2a* or for *sema-2a sema-2b* lived until 48 hr after eclosion, and we thus examined PN dendrite targeting in young mutant animals as soon as they eclosed.

We first examined targeting of DL1 PNs, which send their dendrites to the dorsolateral corner of the antennal lobe in a Sema-1a dependent fashion (Komiyama et al., 2007). We used the MARCM strategy (Lee and Luo, 1999) to generate a singly labeled DL1 cell in *sema-2a*$^{-/-}$, *sema-2b*$^{-/-}$, or *sema-2a*$^{-/-}$ *sema-2b*$^{-/-}$ double mutant animals. In *sema-2a*$^{-/-}$ or *sema-2b*$^{-/-}$ single mutant animals, DL1 PN dendrites converged onto the correct glomerulus (Figures 3A–3C) with no obvious defect. However, in *sema-2a*$^{-/-}$ *sema-2b*$^{-/-}$ double mutant animals, DL1 PN dendrites split between the correct dorsolateral side and the opposing ventromedial side (Figure 3D$_1$), or entirely shifted ventromedially (Figure 3D$_2$). Consistent with more widespread targeting deficits in these whole animal mutants, overall antennal lobe morphology was also disrupted and glomerular borders were no longer easily distinguishable.

We quantified the DL1 targeting defect using the distribution of fluorescence intensity across the antennal lobe as previously described (Komiyama et al., 2007). We divided the antennal lobe into 10 bins along the dorsolateral-ventromedial axis, quantified the proportion of dendritic fluorescence in each bin, and plotted the distribution as a histogram. DL1 PN dendrites exhibited a significant ventromedial shift in *sema-2a*$^{-/-}$ *sema-2b*$^{-/-}$ mutant animals compared with wild-type (WT) (Figure 3E). By contrast, we did not find a statistically significant difference between WT and mutant along the orthogonal dorsomedial-ventrolateral axis (Figure 3F).

To extend this analysis to other dorsolateral-targeting PNs, we examined dendrite targeting of three other classes: DL3, DA1 and VA1d. DL3 PNs were labeled using *HB5-43-GAL4*, while DA1 and VA1d were simultaneously labeled using *Mz19-GAL4*. Similar to DL1, these three dorsolateral-targeting PN classes also exhibited significant ventromedial dendrite mistargeting in the absence of both Sema-2a and Sema-2b (Figures 3G–3L). However, we also found significant ventrolateral shifts along the orthogonal axis (Figures 3I and 3L), indicating that dendrites of these PN classes are mistargeted more toward ventral than medial in the absence of Sema-2a/2b. These PN classes target dendrites to more anterior parts of the antennal lobe than DL1 PNs, and the semaphorin gradients were most evident in the posterior parts of the antennal lobe (see Experimental Procedures) where dendrites of DL1 PNs reside. These factors may explain our finding that in the absence of Sema-2a/2b, mistargeting of DL1 PNs best follows the dorsolateral-ventromedial axis.

Since PlexA is a receptor for Sema-1a when Sema-1a acts as a ligand (Winberg et al., 1998b), and PlexB is a receptor for Sema-2a and Sema-2b (Wu et al., 2011), we also tested whether PlexA and PlexB are involved in PN dendrite targeting. We found that pan-neuronal *PlexA* RNAi, which markedly reduces PlexA protein in the antennal lobe and results in severe ORN axon targeting defects (Sweeney et al., 2007), did not affect DL1 PN targeting (Figures S3A–S3C). Likewise, Mz19$^+$ PNs targeted normally in homozygous *plexB* mutant animals (Figures S3D–S3F). These experiments suggest that neither PlexA nor PlexB is required for dorsolateral dendrite targeting. These data do not rule out the possibility that PlexA and PlexB act redundantly. However, these two plexins only share 35% identity, and have distinct ligand binding specificity and intracellular signaling mechanisms (Ayoob et al., 2006).

Taken together, our data indicate that Sema-2a and Sema-2b function redundantly to restrict dendrites of PNs targeting the dorsolateral antennal lobe. Given the enrichment of Sema-2a/2b protein in the ventromedial antennal lobe, they most probably act as repellents for dorsolateral-targeting PN dendrites.

PNs and Degenerating Larval ORNs Produce Sema-2a and Sema-2b

Next, we attempted to determine the cellular source(s) that produce Sema-2a/2b in the ventromedial antennal lobe. We

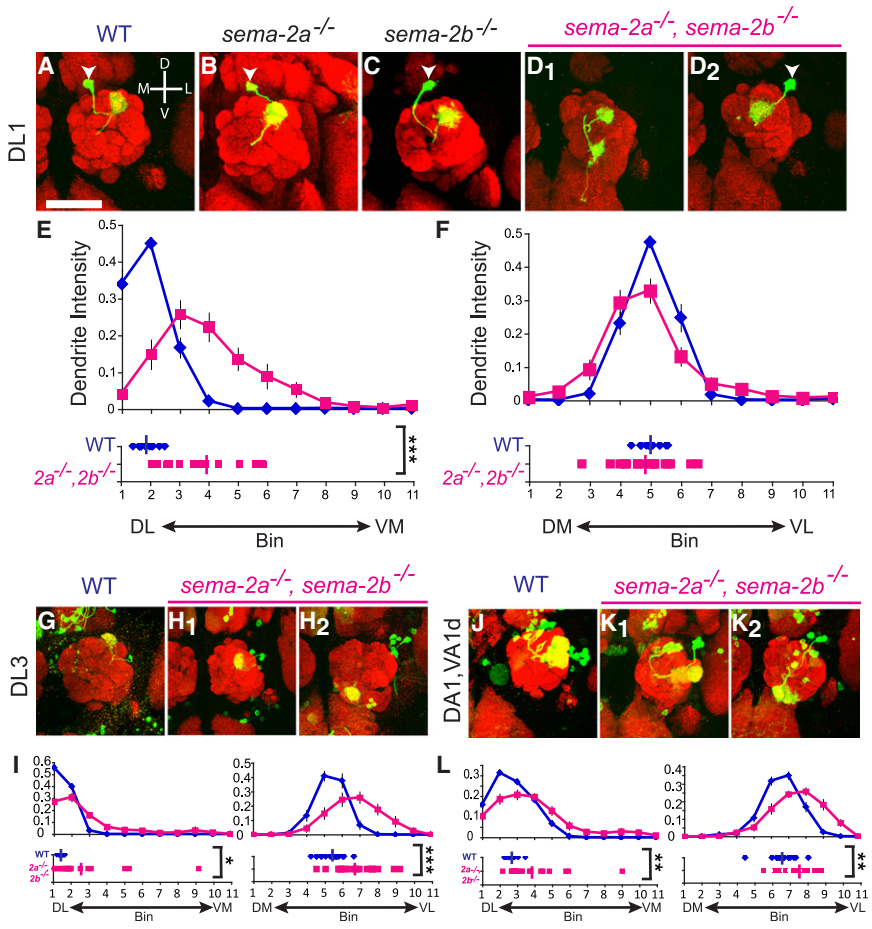

Figure 3. Projection Neuron Dendrite Targeting in *sema-2a sema-2b* Mutant Flies

(A–D) DL1 PN dendrites target normally to the dorsolateral DL1 glomerulus in WT (A) and *sema-2a*$^{-/-}$ (B) or *sema-2b*$^{-/-}$ (C) mutants. In *sema-2a*$^{-/-}$ *sema2b*$^{-/-}$ double mutants, DL1 dendrites split their dendrites between DL1 and an ectopic ventromedial position (D_1) or shift the entire glomerulus ventromedially (D_2). Green, *GH146-GAL4* driven mCD8GFP in MARCM DL1 single cell clones. Red, synaptic marker nc82. Arrowheads: DL1 PN cell bodies. Scale bar represents 50 μm.

(E and F) Quantification of DL1 PN dendrite targeting along the dorsolateral to ventromedial (E) and dorsomedial to ventrolateral axis (F). The antennal lobe is divided into 11 bins with bin 1 being most dorsolateral (E) or most dorsomedial (F) (see Komiyama et al., 2007). The fraction of total dendritic fluorescence in each bin is calculated for WT (blue) and *sema-2a/2b*$^{-/-}$ double mutants (magenta). A scatter plot of the mean dendritic bin position of each antennal lobe is shown below for each condition. n = 11 for WT and *sema-2a/2b*$^{-/-}$ mutants. Error bars represent standard error of the mean. Average positions: E: WT, 1.87 ± 0.09; *sema-2a/2b*$^{-/-}$, 3.95 ± 0.31. F: WT, 5.02 ± 0.10; *sema-2a/2b*$^{-/-}$, 4.85 ± 0.23. ***p < 0.001 by equal variance two-tailed t test.

(G and H) WT DL3 PN dendrites target the dorsolateral DL3 glomerulus (G). In *sema-2a/2b*$^{-/-}$ double mutants, DL3 dendrites mistarget ventrally or ventromedially (H). Green, *HB5-43-GAL4* driven mCD8GFP. Red, synaptic marker nc82.

(I) Quantification of DL3 dendrite mistargeting along the DL-VM (left) and DM-VL (right) axis for WT (blue) and *sema-2a*$^{-/-}$ *sema2b*$^{-/-}$ double mutants (magenta). Average positions along DL-VM axis (left): WT: 1.45 ± 0.02, n = 20; *sema-2a/2b*$^{-/-}$: 2.59 ± 0.45, n = 19. *p < 0.05 by equal variance two-tailed t test. Average positions along DM-VL axis (right): WT: 5.36 ± 0.13, n = 20; *sema-2a/2b*$^{-/-}$: 6.75 ± 0.28, n = 19. ***p < 0.001 by equal variance two-tailed t test.

(J and K) WT VA1d and DA1 PN dendrites target the dorsolateral VA1d and DA1 glomeruli (J). Dendrites shift ventrally or ventromedially in *sema-2a*$^{-/-}$ *sema2b*$^{-/-}$ double mutants (K) antennal lobes. Green, *Mz19-GAL4* driven mCD8GFP. Red, synaptic marker nc82.

(L) Quantification of VA1d+DA1 dendrite mistargeting along the DL-VM (left) and DM-VL (right) axis for WT (blue) and *sema-2a/2b*$^{-/-}$ double mutants (magenta). Average positions along DL-VM axis (left): WT: 2.7 ± 0.08, n = 19; *sema-2a/2b*$^{-/-}$: 3.83 ± 0.37, n = 19. **p < 0.01 by equal variance two-tailed t test. Average positions along DM-VL axis (right): WT: 6.59 ± 0.16, n = 19; *sema-2a/2b*$^{-/-}$: 7.52 ± 0.21, n = 19. **p < 0.01 by equal variance two-tailed t test.

Either full (A–D) or partial (G, H, J, and K) confocal stacks are shown. D, dorsal; V, ventral; M, medial; L, lateral. Figure S3 shows that neither panneural *PlexA* knockdown nor whole animal *PlexB* loss-of-function affects dorsolateral dendrite targeting.

utilized a panel of cell-specific GAL4 drivers to express Sema-2a/2b RNAi in several candidate cell sources and used antibody staining to test the effect of the knockdown. While we found an effective UAS-*sema-2a* RNAi line (see below), none of the UAS-*sema-2b* RNAi lines we tested from a variety of sources significantly reduced Sema-2b antibody staining (data not shown). We thus focused our analysis below on Sema-2a.

We found that neurons rather than glia produced Sema-2a. Pan-neuronal *C155-GAL4*-driven *sema-2a* RNAi almost completely abolished Sema-2a protein staining in the antennal lobe (Figures 4A, 4B and 4E), whereas pan-glial *Repo-GAL4*-driven RNAi had no effect (data not shown). To further determine which types of neurons produce Sema-2a, we first used *GH146-GAL4*, which is expressed in the majority of PNs, to knockdown Sema-2a. This significantly reduced Sema-2a immunostaining in the antennal lobe neuropil (Figures 4C and 4E), as well as in PN cell bodies (Figure 4F). PN-specific knockdown preferentially reduced Sema-2a in the medial antennal lobe, where PN dendrites were most dense (Figure 4C). PNs are therefore a significant source of Sema-2a in the developing antennal lobe.

The adult-specific antennal lobe is adjacent and dorsolateral to the larval-specific antennal lobe (Figure S2; Jefferis et al., 2004) used for larval olfaction (Stocker, 2008). Cellular elements that contribute to the larval antennal lobe include axons of larval-specific ORNs that undergo degeneration and embryonically-born PNs that remodel their dendrites during early pupal development (Marin et al., 2005). Larval ORN axons degenerated during the first 18 hr APF, when adult PN dendrites are actively making targeting decisions (Figure S4). Given that Sema-2a was concentrated in the ventromedial areas of the developing adult antennal lobe during the early pupal stage (Figure S2), we examined whether degenerating larval ORNs contribute

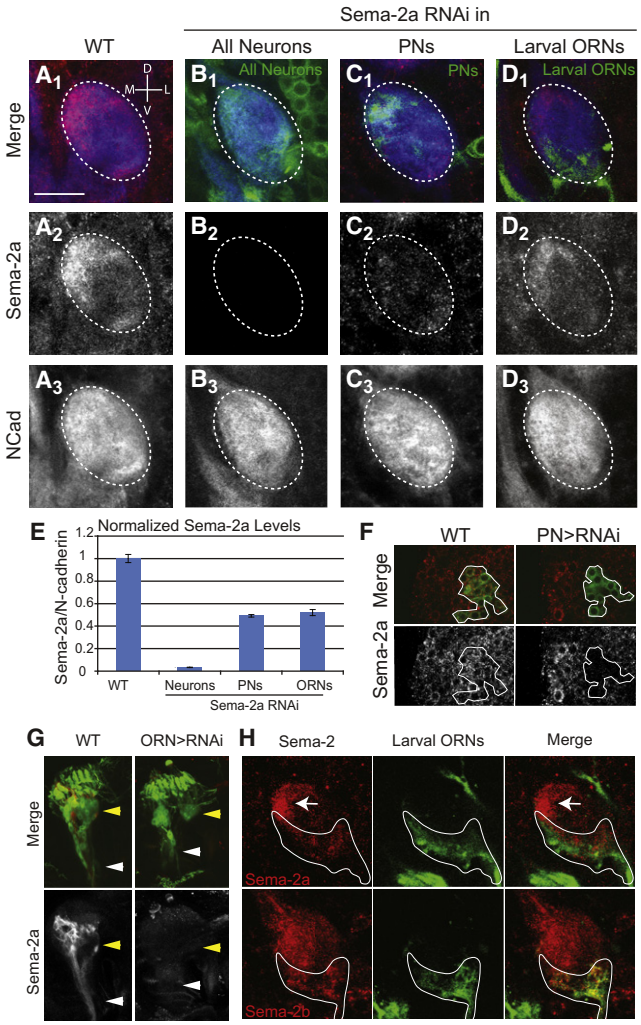

Figure 4. Cellular Source for Sema-2a and Sema-2b

(A) At 16 hr APF, Sema-2a is present in the ventromedial antennal lobe (A_2) while N-cadherin is more broadly distributed (A_3). Antennal lobe is indicated by white dotted outline. Scale bar, 50 μm.

(B) Pan-neuronal knockdown of Sema-2a results in a loss of Sema-2a staining (B_2) while N-cadherin is largely unaffected (B_3). *C155-GAL4* was used to drive UAS-Sema-2a RNAi and UAS-mCD8GFP.

(C) PN knockdown of Sema-2a decreases Sema-2a staining in the medial antennal lobe (C_2) while N-cadherin is largely unaffected (C_3). *GH146-GAL4* was used to drive UAS-Sema-2a RNAi and UAS-mCD8GFP.

(D) Larval ORN knockdown of Sema-2a decreases Sema-2a staining in the ventromedial-ventral antennal lobe (D_3) while N-cadherin is largely unaffected (D_4). *pebbled-GAL4* was used to drive UAS-Sema-2a RNAi and UAS-mCD8GFP.

(E) Quantification of normalized Sema-2a levels with RNAi knockdown (see Experimental Procedures for detail). Average level, standard error of the mean, and n for each condition are as follows: WT: 1.0 ± 0.15, n = 17; C155-driven RNAi: 0.03 ± 0.005, n = 6; GH146-driven RNAi: 0.49 ± 0.01, n = 10; Peb-driven RNAi: 0.52 ± 0.03, n = 10.

(F) At 16 hr APF, PN cell bodies express Sema-2a. The PN-specific *GH146-GAL4* was used to either drive UAS-mCD8GFP alone (left, solid outline) or in combination with UAS-Sema-2a RNAi (right, solid outline). All Sema-2a staining is greatly diminished from PN cell bodies that express UAS-Sema-2a RNAi.

(G) At the third-instar larval stage, ORN cell bodies (yellow arrowhead) and axons (white arrowhead) in the dorsal organ express Sema-2a. The ORN-specific *pebbled-GAL4* was used to either drive UAS-mCD8GFP alone (left) or in combination with UAS-Sema-2a RNAi (right). All Sema-2a staining is greatly diminished from ORN cell bodies and axons that express UAS-Sema-2a RNAi.

(H) At 12 hr APF, Sema-2a (top) and Sema-2b (bottom) proteins coincide with larval ORN axons and terminals labeled by *pebbled-Gal4* driven UAS-mCD8GFP, green (outlined in white). Sema-2a/Sema-2b, red.

Figure S4 shows a time course of ORN axon degeneration between 0 and 16 APF.

Sema-2a at the time of PN target selection. The *pebbled-GAL4* driver is expressed in larval and adult ORNs, but at 16 hr APF, pioneer adult ORN axons have not yet reached the developing antennal lobe. When we drove *sema-2a* RNAi using *pebbled-GAL4*, we found a significant decrease in Sema-2a protein levels in the developing adult antennal lobe at 16hr APF (Figures 4D and 4E). This reduction was most apparent in the ventromedial antennal lobe, the most concentrated site of degenerating larval ORN axons (Figures 4D and S4). Consistent with the notion that larval ORN axons produce Sema-2a in the larval antennal lobe, we found that Sema-2a protein was present in the cell bodies as well as proximal axons of larval ORNs, and that *pebbled-GAL4* driven *sema-2a* RNAi largely eliminated Sema-2a protein staining in larval ORNs (Figure 4G). Together, these data indicate that Sema-2a is produced by larval ORNs, is transported along their axons, and contributes significantly to Sema-2a protein distribution at the ventromedial adult antennal lobe.

Although we were unable to probe the source of Sema-2b with RNAi, we found that Sema-2b protein was enriched in the degenerating larval antennal lobe and the larval ORN axon bundle similar to Sema-2a (Figure 4H and S2). These data indicate that larval ORNs also produce Sema-2b.

Larval ORN Ablation Causes Ventromedial Shift of Dorsolateral-Targeting PN Dendrites

Given that larval ORNs are positioned on the ventromedial side of the developing antennal lobe (Figure S4) and express Sema-2a and Sema-2b, we sought to determine whether cues provided by larval ORNs were necessary for PN dendrite targeting. We utilized an ORN-specific *Or83b-GAL4* in combination with a temperature sensitive GAL80 to drive expression of diphtheria toxin and thus specifically ablate larval ORNs (Figure 5A, left). When flies were grown at 18°C, toxin was minimally expressed due to inhibition of GAL4 by $GAL80^{ts}$, and all larval ORNs survived (Figure 5A, right). When flies were shifted to 29°C as embryos and then returned to 18°C upon pupation, toxin was expressed in larval ORNs and as a result, all larval ORNs were killed (Figure 5A, right).

We examined the effects of larval ORN ablation on the targeting of DA1 and VA1d PN dendrites labeled by a GAL4-independent transgene *Mz19-mCD8-GFP*. In the absence of the toxin transgene, flies grown at 18°C or 29°C exhibited similar dendrite targeting patterns (Figure 5C). When larval ORNs were ablated by toxin expression at the embryonic and larval stage, $Mz19^{+}$ PN dendrites exhibited a marked ventromedial shift (Figure 5B; quantified in Figure 5C), a phenotype similar to that of *sema-2a*$^{-/-}$ *sema-2b*$^{-/-}$ mutants (Figures 3J–3L). Even when grown at 18°C, the presence of the toxin transgene caused a significant

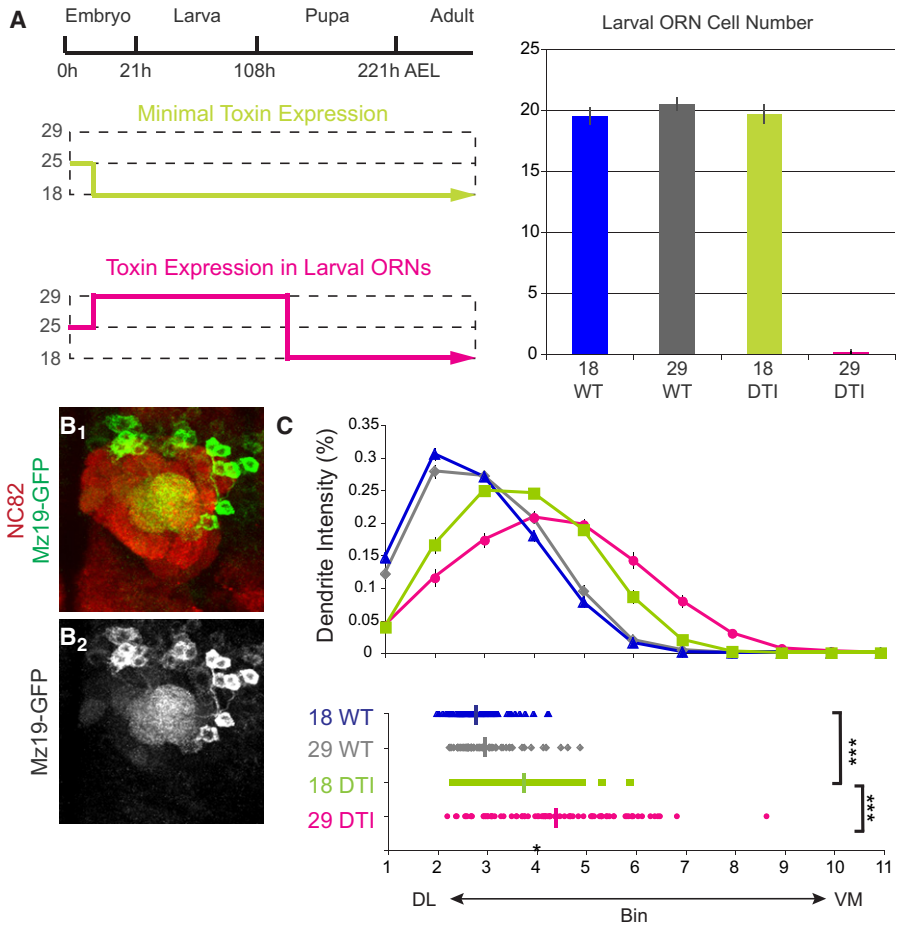

Figure 5. Ablation of Larval ORNs Causes a Ventromedial Shift of PN Dendrites

(A) The ORN-specific *Or83b-GAL4* was used to drive *UAS-diphtheria toxin* (*DTI*) in ORNs in the presence of a temperature sensitive GAL80^{ts} transgene. Flies were raised at 18°C with minimal toxin expression (top left; GAL80 active and therefore GAL4 inactive) or at 29°C from 2 hr after egg laying to 0–1 hr APF (bottom left; GAL80 inactive and therefore GAL4 active during embryonic and larval stages). The right panel shows that animals raised at 29°C during embryonic and larval stages lost their larval ORNs, whereas animals raised at 18°C in the presence of the *DTI* transgene had the same number of larval ORNs compared to animals without the *DTI* transgene.

(B) Representative image to show that ablation of larval ORNs causes MZ19^{+} PN dendrites to mistarget ventromedially (compare with Figure 3J). Mz19-mCD8GFP is shown in green in B_1 and alone in B_2. nc82 staining is shown in red in B_1.

(C) Quantification of MZ19^{+} PN dendrite targeting for the four conditions as indicated (see Figure 3E legend). Average positions: 18°C WT: 2.78 ± 0.06, n = 68; 29°C WT: 2.95 ± 0.07, n = 69; 18°C DTI: 3.73 ± 0.09, n = 78; 29°C DTI: 4.36 ± 0.14, n = 83. ***p < 0.001 by equal variance two-tailed t test.

ventromedial shift of Mz19^{+} PN dendrites relative to no-toxin controls, although this phenotype was not as severe as in 29°C experiments (Figure 5C). This may be because low-level toxin expression at 18°C in the presence of GAL80^{ts}, while insufficient to kill larval ORNs, still perturbed their function, including their ability to produce targeting cues for adult PNs. The essential role for larval ORNs in PN dendrite targeting is evident from the significant difference between the dendrite targeting defects at the two temperatures.

Sema-2a Knockdown in ORNs Causes Ventromedial Shift of Dorsolateral-Targeting PN Dendrites

To test whether Sema-2a derived from larval ORNs is necessary for dendrite targeting of dorsolateral-targeting PNs, we next asked whether RNAi knockdown of Sema-2a in ORNs affected PN dendrite position. Because Sema-2a and Sema-2b function redundantly (Figure 3), *sema-2a* loss-of-function alone should not cause PN dendrite mistargeting. We thus performed Sema-2a RNAi knockdown in *sema-2b*$^{-/-}$ mutant animals using the ORN-specific *pebbled-GAL4* driver. We additionally included one mutant copy of *sema-2a* to reduce the amount of Sema-2a and sensitize the animals to RNAi knockdown. Flies heterozygous for *sema-2a* and *sema-2b* exhibited no dendrite targeting defects (Figures 6A and 6D, compared to Figure 3J). Flies homozygous mutant for *sema-2b* and heterozygous for *sema-2a* exhibited a small but significant ventromedial shift of Mz19^{+} PN dendrite targeting (Figures 6B and 6D). However, when Sema-2a was additionally knocked down in ORNs, we found an additional significant ventromedial shift for Mz19^{+} PN dendrites (Figures 6C and 6D).

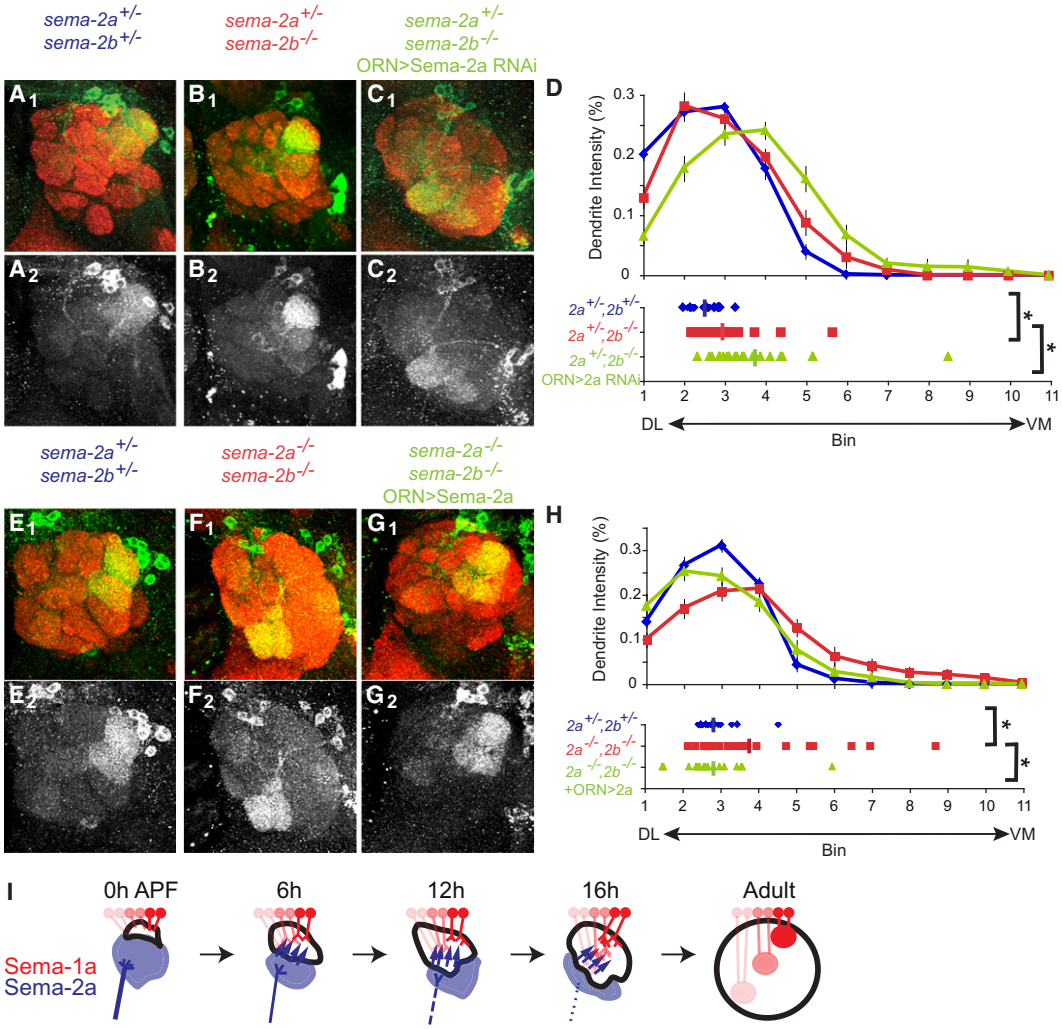

Figure 6. ORN-Specific Knockdown and Rescue

(A) In *sema-2a*$^{-/+}$ *sema-2b*$^{-/+}$ double heterozygous flies raised at 29°C, Mz19^{+} PNs target their dendrites to the correct DA1+VA1d glomeruli in the dorsolateral antennal lobe.

(B) In *sema-2a*$^{-/+}$ *sema-2b*$^{-/-}$ flies, Mz19^{+} PNs largely maintain their normal dorsolateral antennal lobe position.

(C) When Sema-2a is knocked down from ORNs in *sema-2a*$^{-/+}$ *sema-2b*$^{-/-}$ flies, Mz19^{+} PNs mistarget ventromedially.

(D) Quantification of Mz19^{+} PN dendrite targeting along the DL-VM axis in *sema-2a*$^{-/+}$ *sema-2b*$^{-/+}$ double heterozygous flies (blue) compared to *sema-2a*$^{-/+}$ *sema-2b*$^{-/-}$ flies without (red) or with (green) ORN > Sema-2a RNAi. Average positions: *sema-2a*$^{-/+}$ *sema-2b*$^{-/+}$: 2.5 ± 0.08, n = 20; *sema-2a*$^{-/+}$ *sema-2b*$^{-/-}$: 2.95 ± 0.17, n = 22; *sema-2a*$^{-/+}$ *sema-2b*$^{-/-}$ with ORN-driven Sema-2a RNAi: 3.73 ± 0.24, n = 25. *p < 0.05; by equal variance two-tailed t test.

(E) In *sema-2a*$^{-/+}$ *sema-2b*$^{-/+}$ double heterozygous flies raised at 25°C, Mz19^{+} PNs target DA1+VA1d in the dorsolateral antennal lobe.

(F) In *sema-2a*$^{-/-}$ *sema-2b*$^{-/-}$ homozygous mutant flies, MZ19^{+} PNs mistarget ventromedially.

(G) With ORN-driven overexpression of Sema-2a, MZ19^{+} PN dendrites target their normal dorsolateral position in *sema-2a*$^{-/-}$ *sema-2b*$^{-/-}$ homozygous mutant flies.

(H) Quantification of Mz19^{+} PN dendrite targeting along the DL-VM axis in flies that are *sema-2a*$^{-/+}$ *sema-2b*$^{-/+}$ (blue), *sema-2a*$^{-/-}$ *sema-2b*$^{-/-}$ (magenta), and *sema-2a*$^{-/-}$ *sema-2b*$^{-/-}$ with ORN-driven Sema-2a overexpression (green). Average positions: *sema-2a*$^{-/+}$ *sema-2b*$^{-/+}$: 2.8 ± 0.11, n = 20; *sema-2a*$^{-/-}$ *sema-2b*$^{-/-}$: 3.77 ± 0.34, n = 24; *sema-2a*$^{-/-}$, *sema-2b*$^{-/-}$ with ORN-driven Sema-2a overexpression: 2.81 ± 0.23, n = 18. *p < 0.05; both by equal variance two-tailed t test.

(A–C) and (E–G) Top row: Green, Mz19-mCD8GFP; Red, synaptic marker nc82. Bottom row: Mz19-mCD8GFP only. (A)–(D) were done at 29°C and (E)–(H) were done at 25°C.

(I) Schematic summary of dorsolateral targeting of PN dendrites. At 0 hr APF, larval ORN axons (dark blue) occupy the larval antennal lobe (blue). As pupal development proceeds from 0–16 hr APF, larval ORNs and the larval antennal lobe degenerate and release Sema-2a/2b (blue arrows). During the same period, PN dendrites extend their processes into the developing adult antennal lobe (black outline). Dendrites of PNs expressing high levels of Sema-1a (dark red) are repelled to the dorsolateral antennal lobe by larval ORN-derived Sema-2 s. The positions of the degenerating larval lobe and source of Sema-2a/2b were according to data presented in Figures S4 and S2, respectively. Figure S5 shows that ORN overexpression of Sema-2a causes a dorsolateral shift of Mz19^{+} PN dendrites.

From this experiment alone, we cannot distinguish whether the ventromedial shift of Mz19$^+$ dendrites is caused by Sema-2a function in larval ORNs, adult ORNs, or both, as both populations express *pebbled-GAL4*. However, several lines of evidence suggest that larval ORNs make a major contribution. First, larval ORNs contributed significantly to the Sema-2a protein distribution pattern in the ventromedial antennal lobe prior to arrival of adult ORN axons (Figures 4D and 4E). Second, adult PN dendrite patterning occurs before arrival of adult ORN axons. Third, ablating larval ORNs caused a ventromedial shift in dendrite targeting, just as in *sema-2a sema-2b* double mutants. Taken together, these experiments strongly suggest that Sema-2a contributed by larval ORNs repels dorsolateral-targeting PNs from the ventromedial antennal lobe.

ORN Overexpression of Sema-2a Rescues Defects of Dorsolateral-Targeting PN Dendrites

To confirm that larval ORN-derived Sema-2a restricts PN targeting to the dorsolateral antennal lobe, we tested whether Sema-2a overexpression in ORNs was sufficient to rescue the mistargeting of normally dorsolateral-targeting PNs. In *sema-2a*$^{-/-}$ *sema-2b*$^{-/-}$ mutant flies, Sema-2a overexpression with *pebbled-GAL4* was sufficient to rescue the ventromedial targeting defects of Mz19$^+$ PN dendrites (Figures 6E–6H), supporting the notion that Sema-2a from larval ORNs plays an essential role in regulating dendrite targeting of adult PNs. Even in WT flies, overexpression of Sema-2a in ORNs caused a slight but statistically significant dorsolateral shift of the Mz19$^+$ PN dendrites (Figure S5), providing additional support that ORN-derived Sema-2a is sufficient to repel PN dendrites dorsolaterally.

PN-Derived Sema-2a and Sema-2b Regulate Dendrite Targeting of Ventromedial- Targeting PNs through Dendrite-Dendrite Interactions

Finally, we examined the function of Sema-2a and Sema-2b in PNs that normally target dendrites to the ventromedial antennal lobe. We focused on VM2 PNs, the only ventromedial-targeting PN classes we can label with a specific GAL4 driver (*NP5103*) (Komiyama et al., 2007). In *sema-2a*$^{-/-}$ or *sema-2b*$^{-/-}$ single mutants, VM2 PN targeting appeared normal compared to controls (Figures 7A–7C). However, in *sema-2a*$^{-/-}$ *sema-2b*$^{-/-}$ double mutant flies, VM2 PNs exhibited significant dorsolateral mistargeting (Figures 7D, quantified in Figure 7E and Figure S6A). These experiments indicate that Sema-2a and Sema-2b also act redundantly to direct ventromedial-targeting PN dendrites to their normal positions.

Next, we attempted to determine the cellular source for this additional function of Sema-2a and Sema-2b. Because we needed to use the GAL4/UAS system to label VM2 PNs, we could not use GAL4/UAS again to ablate larval ORNs or perform tissue specific knockdown and rescue as we did for MZ19$^+$ PNs. However, since PNs themselves made a significant contribution to Sema-2a expression (Figures 4E and 4F), and because ventromedial-targeting PNs should express high levels of Sema-2a and Sema-2b given their distribution patterns (Figure 2), we tested whether PN-derived Sema-2a and Sema-2b contribute to VM2 dendrite targeting. We used *NP5103-GAL4* based MARCM to label anterodorsal neuroblast clones from which VM2 PNs are derived (Jefferis et al., 2001). When we induced MARCM neuroblast clones in early larvae such that Sema-2a and Sema-2b were eliminated from all larval-born PNs in the anterodorsal lineage, including VM2 PNs (Figure 7F, left), VM2 PN dendrites exhibited significant dorsolateral mistargeting (Figure 7H, compared with Figure 7G; quantified in Figure 7J and Figure S6B). In contrast, dorsolateral-targeting DL1 PN dendrites were unaffected by removal of Sema-2a/2b from this same neuroblast lineage (Figure S7). These experiments indicate that Sema-2a/2b derived from PNs are essential for VM2 dendrite targeting but not for DL1 dendrite targeting.

PN-derived Sema-2a and Sema-2b can affect VM2 dendrite targeting through two mechanisms. First, they could act cell-autonomously, for example by modifying the cell surface presentation of a targeting receptor. Second, they could act cell-nonautonomously as ligands to mediate dendrite-dendrite interactions among PNs. To distinguish between these two possibilities, we took advantage of the fact that VM2 PNs are produced late in the anterodorsal lineage, and induced smaller MARCM neuroblast clones that contained VM2 PNs but few other PNs within the same lineage (Figure 7F, right). We found that VM2 dendrite targeting in these smaller *sema-2a*$^{-/-}$ *sema-2b*$^{-/-}$ neuroblast clones was largely normal (Figure 7I, quantified in Figure 7J). Thus, Sema-2a/2b act nonautonomously for VM2 dendrite targeting. The significant differences between VM2 targeting in large and small neuroblast clones (Figure 7J) indicate that Sema-2a/2b produced by early-born PNs in the same anterodorsal neuroblast lineage regulate late-born VM2 PN dendrite targeting.

DISCUSSION

The graded distribution of Sema-1a on PN dendrites provided the first identified instructive mechanism at the cell surface for PN dendrite targeting (Komiyama et al., 2007). Although Semaphorins predominantly act as repulsive axon guidance ligands (Tran et al., 2007), transmembrane Sema-1a acts cell-autonomously as a receptor to instruct PN dendrite targeting along the dorsolateral-ventromedial axis of the antennal lobe (Komiyama et al., 2007), and to regulate wiring of the *Drosophila* visual system (Cafferty et al., 2006). This raises two important questions for the wiring of the olfactory circuit: what are the spatial cues for Sema-1a-dependent PN dendrite targeting, and which cells provide these cues to initiate patterning events that eventually give rise to the exquisite wiring specificity of this circuit? Here we present evidence that secreted semaphorins produced by degenerating larval ORNs provide an important source for this patterning (Figure 6I). Our study provides insights into axon-to-dendrite interactions in neural circuit assembly, and suggests a new Semaphorin signaling mechanism.

Sema-2a and Sema-2b Provide Spatial Cues for Sema-1a-Dependent Dorsolateral-Targeting PN Dendrites

Several lines of evidence suggest that secreted Sema-2a/2b provide instructive spatial cues for Sema-1a-dependent dorsolateral-targeting PN dendrites. First, Sema-1a-Fc binds specifically to Sema-2a-expressing imaginal disc epithelial cells and

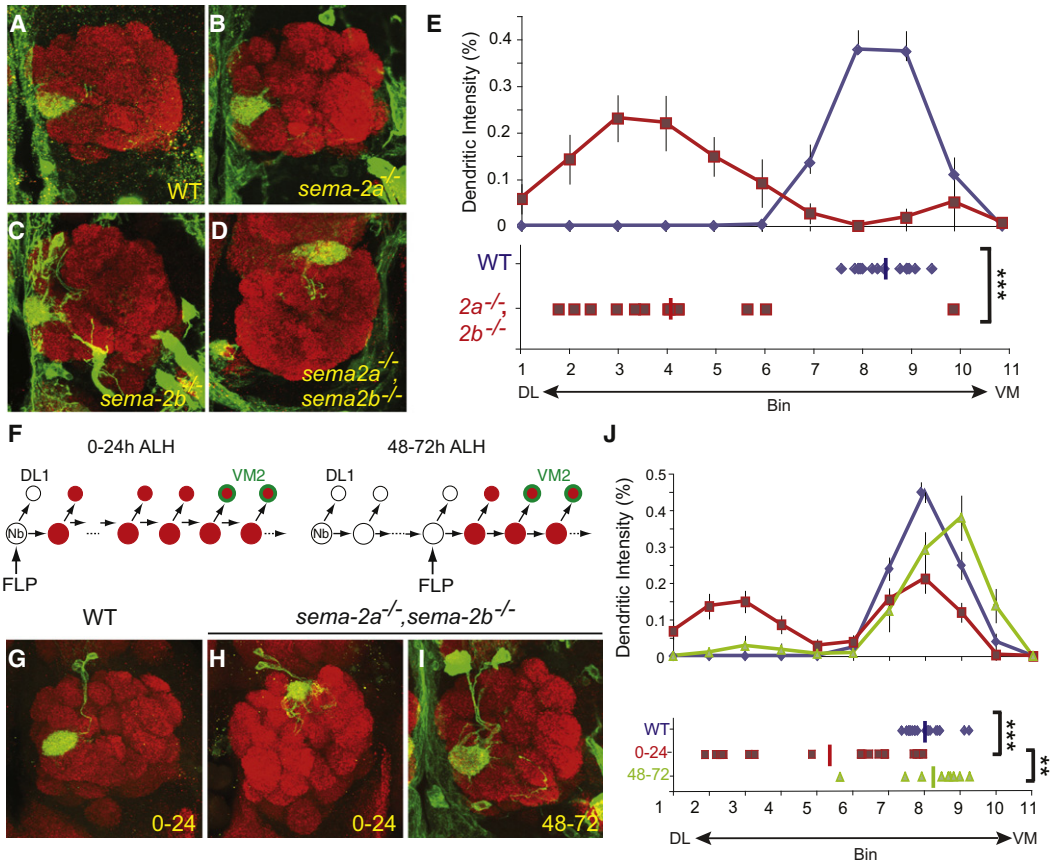

Figure 7. Sema-2a and Sema-2b Function in PNs to Regulate Dendrite Targeting to Ventromedial Antennal Lobe

(A–D) VM2 PN dendrites target normally to the ventromedial VM2 glomerulus in WT (A) and *sema-2a*$^{-/-}$ (B) or *sema-2b*$^{-/-}$ (C) mutants. In *sema-2a/2b*$^{-/-}$ double mutants, VM2 dendrites shift dorsolaterally (D). Green, *NP5103-GAL4* driven mCD8GFP. Red, synaptic marker nc82. Partial confocal stacks are shown. *NP5103-GAL4* is also expressed in some cells and processes outside the antennal lobe.

(E) Quantification of VM2 dendrite mistargeting along the DL-VM axis for WT (blue) and *sema-2a*$^{-/-}$ *sema-2b*$^{-/}$ double mutants (magenta). Average positions along DL-VM axis (left): WT: 8.45 ± 0.15, n = 14; *sema-2a/2b*$^{-/-}$: 4.17 ± 0.59, n = 13. ***p < 0.001 by equal variance two-tailed t test.

(F) Schematic of the MARCM strategy to generate anterodorsal neuroblast clones that are mutant for *sema-2a* and *sema-2b* while simultaneously labeling VM2 PNs. MARCM clones were induced by activating FLP recombinase either between 0-24h after larval hatching (ALH) or between 48-72h ALH. The early induction protocol (left) causes all larval-born PNs except the first DL1 PN to be *sema-2a*$^{-/-}$ *sema-2b*$^{-/-}$ (red) (Jefferis et al., 2001). The late induction protocol (right) produces only a small subset of *sema-2a*$^{-/-}$ *sema-2b*$^{-/-}$ PNs. In either case, two to three VM2 PNs within the neuroblast clone are *sema-2a*$^{-/-}$ *sema-2b*$^{-/-}$ and are labeled by *NP5103-GAL4* driven UAS-mCD8GFP (green).

(G–I) In WT anterodorsal neuroblast clones generated between 0–24 hr ALH, VM2 PN dendrites target normally to the ventromedial VM2 glomerulus (G). In *sema-2a*$^{-/-}$ *sema-2b*$^{-/-}$ double mutant PN anterodorsal neuroblast clones generated between 0–24 hr ALH, VM2 dendrites shift dorsolaterally (H). In contrast, in *sema-2a*$^{-/-}$ *sema-2b*$^{-/-}$ double mutant PN anterodorsal neuroblast clones generated between 48–72 hr ALH, VM2 dendrites target normally (I). Green, *NP5103-GAL4* driven mCD8GFP in an anterodorsal neuroblast clone. Red, synaptic marker nc82. Partial confocal stacks are shown.

(J) Quantification of VM2 dendrite mistargeting along the DL-VM axis for WT (blue) and *sema-2a/2b*$^{-/-}$ double mutant MARCM neuroblast clones generated at 0–24 hr (magenta) or 48–72 hr ALH (green). Average positions along DL-VM axis: WT 0–24 hr: 8.04 ± 0.11, n = 21; *sema-2a/2b*$^{-/-}$ 0–24 hr: 5.41 ± 0.48, n = 23; *sema-2a/2b*$^{-/-}$ 48–72 hr: 8.23 ± 0.37, n = 9. ***p < 0.001; **p < 0.01; equal variance two-tailed t test.

Figure S6 shows quantification of VM2 dendrite distribution along the orthogonal dorsomedial-ventrolateral axis. Figure S7 shows that dorsolateral DL1 dendrite targeting is not affected by loss of PN-derived Sema-2a/2b in the same lineage.

brain neurons (Figures 1 and S1). Second, Sema-2a/2b and Sema-1a show opposing expression patterns in the developing antennal lobe. Sema-1a exhibits a high dorsolateral-low ventromedial gradient (Komiyama et al., 2007), whereas Sema-2a and Sema-2b exhibit the opposite gradient (Figure 2). Third, loss of Sema-2a and Sema-2b results in a ventromedial shift of dorsolateral-targeting PN dendrites (Figure 3), a phenotype qualitatively similar to that of single cell Sema-1a knockout in these PNs (Komiyama et al., 2007). The opposing patterns of expression but similar loss-of-function phenotypes suggest that Sema-2a/2b act as repulsive cues for Sema-1a-expressing PN dendrites.

Intriguingly, the binding of Sema-2a to Sema-1a appears to be conditional and may be indirect. We failed to detect direct binding of purified Sema-1a to Sema-2a protein in vitro, binding of Sema-2a-Fc to Sema-1a-expressing cells in vivo, or binding of

Sema-1a-Fc to membrane-tethered Sema-2a expressed in S2 or BG2 cells (data not shown). Several possibilities may reconcile these negative data with the binding of Sema-1a-Fc to Sema-2a-expressing cells in vivo (Figure 1 and S1). First, Sema-2a may require a specific modification that confers Sema-1a binding capacity. If so, Sema-2a is modified correctly in *Drosophila* neurons and wing disc cells, but not in S2 cells, BG2 cells, or the Hi5 cells we used to produce Sema-2a-Fc for in vitro assays. Second, Sema-2a may bind Sema-1a with low affinity, such that only highly concentrated or clustered Sema-2a will exhibit detectable Sema-1a binding. Third, Sema-1a/Sema-2a binding may require a cofactor in the Sema-2a-expressing cell. This cofactor may be present in *Drosophila* neurons and wing disc cells but absent from S2 or BG2 cells. Finally, Sema-2a expression may activate a different molecule that in turn binds directly to Sema-1a and serves as a ligand. These possibilities are not mutually exclusive. The fact that Sema-1a binds more strongly to cells expressing membrane-tethered Sema-2a than secreted Sema-2a suggests that Sema-2a acts on the cell surface, and therefore favors the possibility that Sema-2a is at least part of the ligand complex. However, definitive demonstration of a receptor-ligand interaction, either direct or indirect involving an unknown coreceptor, would require additional biochemical data.

Notably, we could not detect Sema-1a-Fc binding to secreted or membrane-tethered Sema-2b-expressing midline neurons, mushroom body neurons or wing disc cells, despite our genetic data indicating that Sema-2a and Sema-2b act redundantly in PN dendrite targeting. Sema-2b expression from the transgene we used to test binding may be too low. Alternatively, Sema-2b may exhibit different biochemical properties compared to Sema-2a, as recently shown in the context of *Drosophila* embryonic axon guidance, where Sema-2a/2b act as ligands for PlexB (Wu et al., 2011). Prior to our study, plexins were the only known extracellular semaphorin binding partners in invertebrates (Winberg et al., 1998b; Wu et al., 2011). However, neither PlexA nor PlexB were required for PN dendrite targeting to the dorsolateral antennal lobe (Figure S3), suggesting that plexins are not involved in mediating the interactions between Sema-1a and Sema-2a/2b, at least for dorsolateral-targeting PNs.

The detailed biochemical mechanisms of how transmembrane and secreted semaphorins cooperate remain to be elucidated in future experiments. However, our study indicates that secreted semaphorins can act as cues for dendrites that express a transmembrane semaphorin receptor. This finding expands on the traditional view of semaphorin-plexin ligand-receptor pairing. Given the large number of secreted and transmembrane semaphorins, especially in the vertebrate nervous system (Tran et al., 2007), our findings raise the possibility that the action of certain semaphorins may be mediated, directly or indirectly, by other transmembrane semaphorins acting as receptors.

Degenerating Axons Instruct Targeting of Developing Dendrites

We provide several lines of evidence that degenerating larval ORN axons are an important source for Sema-2a/2b to instruct Sema-1a-dependent PN dendrite targeting (Figure 6I). First, Sema-2a and Sema-2b are produced in larval ORNs and are present in their axon terminals. Second, Sema-2a and Sema-2b are most concentrated in the ventromedial antennal lobe, at the boundary between degenerating larval antennal lobe and developing adult antennal lobe. Third, knocking down Sema-2a in larval ORNs significantly reduces Sema-2a protein in the developing antennal lobe. Fourth, larval ORN ablation causes a ventromedial shift of dorsolateral-targeting PN dendrites, a phenotype similar to that of *sema-2a*$^{-/-}$ *sema-2b*$^{-/-}$ mutants. Fifth, ORN-specific Sema-2a knockdown in a *sema-2b* mutant background causes a significant ventromedial shift. Sixth, expressing Sema-2a only in ORNs is sufficient to rescue PN mistargeting phenotypes in *sema-2a*$^{-/-}$ *sema-2b*$^{-/-}$ double mutants. Due to technical limitations, we cannot strictly determine in the last two experiments whether larval ORNs, adult ORNs, or both contribute to the knockdown or rescue effects. However, given that adult ORNs arrive at the antennal lobe after the coarse PN map has already formed, and given the similar phenotypes between ORN-specific Sema-2a knockdown (Figure 6) and larval ORN ablation (Figure 5), we propose that degenerating larval ORNs provide a major source of secreted semaphorins to direct the dendrite targeting of adult PNs.

Protein gradients usually align with major body axes (St Johnston and Nüsslein-Volhard, 1992), possibly reflecting earlier developmental patterning events. Why does the Sema-1a protein gradient orient along a slanted dorsolateral-ventromedial axis? Our finding that ventromedially-located larval ORNs produce targeting cues for adult PNs offers a satisfying explanation for the orientation of the Sema-1a gradient.

To our knowledge, this study provides the first example of a degenerating structure that provides instructive cues to pattern a developing neural circuit. This strategy can be widely used in animals that undergo metamorphosis, such as holometabolic insects and amphibians, where nervous systems undergo large-scale changes. Even in animals that do not undergo metamorphosis, regressive events such as axon pruning and synapse elimination are prevalent during development (Luo and O'Leary, 2005; Sanes and Lichtman, 1999). Regressive events also occur in certain parts of the nervous system that undergo constant replacement, such as mammalian olfactory receptor neurons and olfactory bulb interneurons. Degenerating structures may also instruct the formation of new structures under some of these circumstances. An advantage of this strategy could be to mechanistically couple regressive and progressive events.

Different Cell Sources of Sema-2a/2b Direct PN Dendrites to Distinct Positions

Interestingly, ventromedial-targeting PN dendrites, which express high levels of Sema-2a and Sema-2b, also require Sema-2a/2b. Sema-2a/2b are not required cell autonomously, as mutant VM2 cells in small neuroblast clones target normally (Figure 7). Notably, removing Sema-2a/2b from larval born PNs of the anterodorsal lineage (including VM2 PNs) is sufficient to cause significant dorsolateral mistargeting, although not as severely as in whole animal mutants (compare red traces in Figures 7E and 7J). PNs derived from the lateral and ventral lineages, PNs born in embryos from the anterodorsal lineage

(Jefferis et al., 2001; Marin et al., 2005) or larval ORNs may contribute additional Sema-2a/2b. Nonetheless, our study demonstrates that dendrite-dendrite interactions contribute to the ventromedial targeting of VM2 PN dendrites: VM2 targeting relies on Sema-2a/2b from other non-VM2 PNs born earlier in the neuroblast lineage. This is conceptually similar to our previous finding that early-arriving antennal axons repel late-arriving maxillary palp axons using Sema-1a as a repulsive ligand (Sweeney et al., 2007). A similar sequential mechanism regulates mouse ORN axon targeting (Takeuchi et al., 2010).

What is the receptor for Sema-2a/2b in VM2 PNs? Given that Sema-1a is not required cell-autonomously for VM2 dendrite targeting (Komiyama et al., 2007), ventromedial-targeting PNs likely use a different receptor, in addition to a different cell source, compared with dorsolateral-targeting PNs. The role of secreted semaphorins in ventromedial-targeting dendrites may be analogous to the attractive function of Sema-2b in embryonic longitudinal axon tract formation, where PlexB serves as the receptor (Wu et al., 2011). PN-derived Sema-2a/2b appear to preferentially affect ventromedial-targeting PNs, as dorsolateral-targeting DL1 PN dendrites are not affected by analogous removal of Sema-2a/2b from PNs (Figure S7).

Taken together, our data suggest that secreted semaphorins from two different cellular sources are differentially responsible for dendrite targeting of dorsolateral- and ventromedial-targeting PNs. These findings reinforce the notion that secreted semaphorins play a general role in determining PN dendrite targeting along the dorsolateral-ventromedial axis, and highlight the diversity of semaphorin signaling mechanisms.

Gradients and Neural Map Formation

Molecular gradients in neuronal wiring were first demonstrated by the use of ephrins/Eph receptors for establishing the vertebrate retinotopic map (Cheng et al., 1995; Drescher et al., 1995). The retinotopic map is a continuous two-dimensional representation of visual space, in which nearby retinal ganglion cells project to nearby tectal targets. The olfactory map is qualitatively different from the visual map in that nearby glomeruli do not necessarily receive projections from nearby ORNs or PNs (Luo and Flanagan, 2007). However, graded protein distributions are used in both the *Drosophila* (Komiyama et al., 2007; this study) and mammalian (Imai et al., 2009; Takeuchi et al., 2010) olfactory systems. In the mammalian olfactory system, semaphorins act as repulsive ligands for the neuropilin receptors to mediate ORN axon-axon interactions (Imai et al., 2009; Takeuchi et al., 2010). We found that graded Sema-2a/2b from degenerating axons instruct Sema-1a-dependent PN dendrite targeting to the dorsolateral antennal lobe, revealing an axon-to-dendrite signaling.

This study expands our understanding of how gradients and countergradients are used to construct neural maps. Protein gradients provide an efficient mechanism for targeting many classes of neurons with minimal types of molecules, at least at a coarse level. The coarse targeting specified by protein gradients can then be refined by additional mechanisms, such as class-specific labeling molecules (Hong et al., 2009; Kaneko-Goto et al., 2008; Serizawa et al., 2006), which further segregate the olfactory circuit into discrete glomeruli.

EXPERIMENTAL PROCEDURES

Mutants and Transgenes

A P-element insertion *sema-2a*^{P2} was used for all *sema-2a* loss-of-function analysis (Ayoob et al., 2006). Two alleles of *sema-2b* were used—a pBac insertion f02042 (Thibault et al., 2004) and FRT-mediated deletion #078 (Sema-2b^{C4}) (Wu et al., 2011). A P-element insertion KG00878 into *PlexB* was used for loss-of-function analysis (Ayoob et al., 2006). UAS-*sema-2a* RNAi transformant ID #15811 was used for all RNAi experiments (VDRC). To label Mz19^{+} PN dendrites, *Mz19-GAL4* or *Mz19-mCD8GFP* were used as previously described (Berdnik et al., 2006). To label DL3 dendrites, the enhancer trap line *HB5-43-GAL4* (kindly provided by U. Heberlein and screened by E.C. Marin) was used. To label VM2 dendrites, *NP5103-GAL4* was used as previously characterized (Komiyama et al., 2007). Other transgenes were from the following sources: *pebbled-GAL4* (Sweeney et al., 2007); *UAS-HA-PlexA* (Terman et al., 2002); *UAS-PlexB* (Ayoob et al., 2006); *UAS-Sema-2a-TM* (Wu et al., 2011); *UAS-Sema-2a* (Winberg et al., 1998a).

Mosaic Analyses

MARCM analysis to label DL1 single cell clones was performed as previously described (Komiyama et al., 2003; Lee and Luo, 1999). In summary, flies were heat shocked for 1 hr at 37°C between 2 and 26 hr after larval hatching. QMARCM labeled DL1 single cell clones (Potter et al., 2010) were similarly generated but were heat shocked for an additional hour to increase clone frequency. VM2 anterodorsal neuroblast clones were generated between 0, 24, 48, and 72 hr after larval hatching and clone frequency was increased by performing two 1-hr heat shocks with 30 min at room temperature in between heat shocks. Additionally, flies were raised at 18°C after heat shocking for 24 hr.

Larval ORN Ablation

Or83b-GAL4 (Larsson et al., 2004), which is expressed in all larval ORNs and ~70%–80% adult ORNs, was used to drive the expression of diphtheria toxin (DTI) (Han et al., 2000). To specifically ablate larval ORNs and leave adult ORNs intact, *tub-GAL80*^{ts} (McGuire et al., 2003) was used to suppress GAL4 expression after puparium formation. Animals were raised at 25°C for 2 hr to allow egg laying and then shifted to 29°C to inactive GAL80, thus allowing GAL4 and DTI expression to ablate all larval ORNs. Animals were shifted back to 18°C at 0 hr APF to activate GAL80 and to allow the survival of adult ORNs.

Immunostaining

Immunostaining was performed according to previously described methods (Sweeney et al., 2007). Mouse anti-Sema-2a (Developmental Studies Hybridoma Bank) was used at a concentration of 1:50. A polyclonal rabbit antibody against the entire Sema-2b protein was commercially generated (Covance), preabsorbed against homozygous mutant *sema-2b* larval brains, and used at a concentration of 1:500. Anti-rabbit Sema-1a antibody (Yu et al., 1998) was used at 1:5000. Anti-rabbit PlexA antibody was used as previously described (Sweeney et al., 2007). Anti-rabbit PlexB antibody was commercially generated (New England Peptide) according to the peptide sequence CRYKNEYDRKKRRADFGD in the extracellular domain of the PlexinB protein, custom affinity-purified, and used at 1:500. Rat anti-N-cadherin (Developmental Studies Hybridoma Bank) was used at the concentration of 1:30. Rat anti-mouse CD8 and mouse monoclonal antibody nc82 were used as previously described (Sweeney et al., 2007).

Sema-1a-Fc protein was generated by Hi5 cell viral infection of a construct containing the extracellular fragment of Sema-1a fused to the human IgG Fc fragment. From the time of supernatant collection, Sema-1a-Fc protein was kept in 0.5 M NaCl. Protein A purification of the Sema-1a-Fc-containing supernatant was then performed: cell supernatant was centrifuged at 1500 rpm for 15 min, filtered once with glass Whatman and then twice with HV filters, and pumped over an ~5–10 ml column packed with FastFlow ProteinA beads at 1.5–2 ml/min. The column was then washed with at least 10 column volumes of PBS adjusted to 0.5M NaCl and eluted with 100 mM Glycine, 0.5M NaCl into 1 M Tris (pH = 8), 0.5 M NaCl. Fc protein concentration was determined using a Nanodrop. Fc protein was kept at 4°C and used within 1 month of generation.

To perform live staining, pupal brains or third-instar larval wing discs were dissected on ice in cold PBS for no longer than 20 min. Sema-1a-Fc protein at a concentration of ~0.5 mg/ml or antibody at three times the concentration used for fixed and permeabilized tissue were diluted in cold PBS and incubated on a nutator with the brains/discs for 1 hr at 4°C in thin wall PCR tubes. Three quick washes with cold PBS were performed followed by fixation for 20 min at room temperature in 4% PFA in PBS. After 20 min of fixation, a squirt of 0.3% PBT was added to prevent tissue adherence to the pipet tip before the fixative was removed. Brains/discs were then washed three times 20 min with 0.3% PBT, blocked for 30 min with 5% NGS in 0.3% PBT, and stained as described for fixed and permeabilized brain tissue (see above).

All images were collected using a Zeiss LSM 510 confocal microscope.

Quantification Procedures

Relative fluorescence quantification of antibody staining and binning quantification of DL1 and Mz19^{+} PN dendrites along the dorsolateral-ventromedial axis was performed as previously described (Komiyama et al., 2007; Sweeney et al., 2007). A specific posterior confocal section was used to quantify Sema-2a/2b protein distribution in 16 hr APF WT pupal brains (Figure 2) as in Komiyama et al. (2007). The presence of an external landmark enabled the identification of the same plane in different brains.

For quantitative comparison of Sema-2a protein levels under different genetic manipulations, the same posterior confocal section as Figure 2 was used. In this single confocal section, the antennal lobe was outlined according to N-cadherin staining and the total fluorescence was calculated within the outlined region for both N-cadherin and Sema-2a by the Zeiss LSM 510 software. Total Sema-2a immunofluorescence was then divided by total N-cadherin to obtain the normalized fluorescence intensity of Sema-2a. Two separate staining experiments were averaged. Because the intensity of staining in WT brains varied between experiments, the percent change from WT was calculated for each experiment. Percent change from WT equals normalized fluorescence for each RNAi condition divided by the normalized WT fluorescence. The average percent change and standard error for each condition is graphed.

SUPPLEMENTAL INFORMATION

Supplemental Information includes seven figures and can be found with this article online at doi:10.1016/j.neuron.2011.09.026.

ACKNOWLEDGMENTS

This work was supported by NIH (R01-DC005982 to L.L., R01-NS35165 to A.L.K.) and the Howard Hughes Medical Institute (to A.L.K., K.C.G., and L.L.). L.B.S. was supported by the Developmental and Neonatal Training Program (T32 HD007249) and a Lieberman Fellowship. We thank N. Goriatcheva and D. Luginbuhl for technical assistance, U. Heberlein and E.C. Marin for an unpublished GAL4 line, and W. Hong for critical comments.

Accepted: September 13, 2011
Published: December 7, 2011

REFERENCES

Ayoob, J.C., Terman, J.R., and Kolodkin, A.L. (2006). Drosophila Plexin B is a Sema-2a receptor required for axon guidance. Development *133*, 2125–2135.

Berdnik, D., Chihara, T., Couto, A., and Luo, L. (2006). Wiring stability of the adult Drosophila olfactory circuit after lesion. J. Neurosci. *26*, 3367–3376.

Brand, A.H., and Perrimon, N. (1993). Targeted gene expression as a means of altering cell fates and generating dominant phenotypes. Development *118*, 401–415.

Cafferty, P., Yu, L., Long, H., and Rao, Y. (2006). Semaphorin-1a functions as a guidance receptor in the Drosophila visual system. J. Neurosci. *26*, 3999–4003.

Cheng, H.-J., Nakamoto, M., Bergemann, A.D., and Flanagan, J.G. (1995). Complementary gradients in expression and binding of ELF-1 and Mek4 in development of the topographic retinotectal projection map. Cell *82*, 371–381.

Drescher, U., Kremoser, C., Handwerker, C., Loschinger, J., Noda, M., and Bonhoeffer, F. (1995). In vitro guidance of a retinal ganglion cell axons by RAGS, a 25kDa tectal protein related to ligands for Eph receptor tyrosine kinase. Cell *82*, 369–370.

Han, D.D., Stein, D., and Stevens, L.M. (2000). Investigating the function of follicular subpopulations during Drosophila oogenesis through hormone-dependent enhancer-targeted cell ablation. Development *127*, 573–583.

Hong, W., Zhu, H., Potter, C.J., Barsh, G., Kurusu, M., Zinn, K., and Luo, L. (2009). Leucine-rich repeat transmembrane proteins instruct discrete dendrite targeting in an olfactory map. Nat. Neurosci. *12*, 1542–1550.

Imai, T., Yamazaki, T., Kobayakawa, R., Kobayakawa, K., Abe, T., Suzuki, M., and Sakano, H. (2009). Pre-target axon sorting establishes the neural map topography. Science *325*, 585–590.

Janssen, B.J., Robinson, R.A., Pérez-Brangulí, F., Bell, C.H., Mitchell, K.J., Siebold, C., and Jones, E.Y. (2010). Structural basis of semaphorin-plexin signalling. Nature *467*, 1118–1122.

Jefferis, G.S., Marin, E.C., Stocker, R.F., and Luo, L. (2001). Target neuron prespecification in the olfactory map of Drosophila. Nature *414*, 204–208.

Jefferis, G.S.X.E., Vyas, R.M., Berdnik, D., Ramaekers, A., Stocker, R.F., Tanaka, N.K., Ito, K., and Luo, L. (2004). Developmental origin of wiring specificity in the olfactory system of Drosophila. Development *131*, 117–130.

Kaneko-Goto, T., Yoshihara, S.-I., Miyazaki, H., and Yoshihara, Y. (2008). BIG-2 mediates olfactory axon convergence to target glomeruli. Neuron *57*, 834–846.

Kolodkin, A.L., Matthes, D.J., and Goodman, C.S. (1993). The semaphorin genes encode a family of transmembrane and secreted growth cone guidance molecules. Cell *75*, 1389–1399.

Komiyama, T., Johnson, W.A., Luo, L., and Jefferis, G.S. (2003). From lineage to wiring specificity. POU domain transcription factors control precise connections of Drosophila olfactory projection neurons. Cell *112*, 157–167.

Komiyama, T., Sweeney, L.B., Schuldiner, O., Garcia, K.C., and Luo, L. (2007). Graded expression of semaphorin-1a cell-autonomously directs dendritic targeting of olfactory projection neurons. Cell *128*, 399–410.

Larsson, M.C., Domingos, A.I., Jones, W.D., Chiappe, M.E., Amrein, H., and Vosshall, L.B. (2004). Or83b encodes a broadly expressed odorant receptor essential for Drosophila olfaction. Neuron *43*, 703–714.

Lee, T., and Luo, L. (1999). Mosaic analysis with a repressible cell marker for studies of gene function in neuronal morphogenesis. Neuron *22*, 451–461.

Liu, H., Juo, Z.S., Shim, A.H., Focia, P.J., Chen, X., Garcia, K.C., and He, X. (2010). Structural basis of semaphorin-plexin recognition and viral mimicry from Sema7A and A39R complexes with PlexinC1. Cell *142*, 749–761.

Luo, L., and O'Leary, D.D. (2005). Axon retraction and degeneration in development and disease. Annu. Rev. Neurosci. *28*, 127–156.

Luo, L., and Flanagan, J.G. (2007). Development of continuous and discrete neural maps. Neuron *56*, 284–300.

Marin, E.C., Watts, R.J., Tanaka, N.K., Ito, K., and Luo, L. (2005). Developmentally programmed remodeling of the Drosophila olfactory circuit. Development *132*, 725–737.

McGuire, S.E., Le, P.T., Osborn, A.J., Matsumoto, K., and Davis, R.L. (2003). Spatiotemporal rescue of memory dysfunction in Drosophila. Science *302*, 1765–1768.

Nogi, T., Yasui, N., Mihara, E., Matsunaga, Y., Noda, M., Yamashita, N., Toyofuku, T., Uchiyama, S., Goshima, Y., Kumanogoh, A., and Takagi, J. (2010). Structural basis for semaphorin signalling through the plexin receptor. Nature *467*, 1123–1127.

Potter, C.J., Tasic, B., Russler, E.V., Liang, L., and Luo, L. (2010). The Q system: a repressible binary system for transgene expression, lineage tracing, and mosaic analysis. Cell *141*, 536–548.

Sanes, J.R., and Lichtman, J.W. (1999). Development of the vertebrate neuromuscular junction. Annu. Rev. Neurosci. *22*, 389–442.

Serizawa, S., Miyamichi, K., Takeuchi, H., Yamagishi, Y., Suzuki, M., and Sakano, H. (2006). A neuronal identity code for the odorant receptor-specific and activity-dependent axon sorting. Cell *127*, 1057–1069.

St Johnston, D., and Nüsslein-Volhard, C. (1992). The origin of pattern and polarity in the Drosophila embryo. Cell *68*, 201–219.

Stocker, R.F. (2008). Design of the larval chemosensory system. Adv. Exp. Med. Biol. *628*, 69–81.

Sweeney, L.B., Couto, A., Chou, Y.-H., Berdnik, D., Dickson, B.J., Luo, L., and Komiyama, T. (2007). Temporal target restriction of olfactory receptor neurons by Semaphorin-1a/PlexinA-mediated axon-axon interactions. Neuron *53*, 185–200.

Takeuchi, H., Inokuchi, K., Aoki, M., Suto, F., Tsuboi, A., Matsuda, I., Suzuki, M., Aiba, A., Serizawa, S., Yoshihara, Y., et al. (2010). Sequential arrival and graded secretion of Sema3F by olfactory neuron axons specify map topography at the bulb. Cell *141*, 1056–1067.

Terman, J.R., Mao, T., Pasterkamp, R.J., Yu, H.H., and Kolodkin, A.L. (2002). MICALs, a family of conserved flavoprotein oxidoreductases, function in plexin-mediated axonal repulsion. Cell *109*, 887–900.

Thibault, S.T., Singer, M.A., Miyazaki, W.Y., Milash, B., Dompe, N.A., Singh, C.M., Buchholz, R., Demsky, M., Fawcett, R., Francis-Lang, H.L., et al. (2004). A complementary transposon tool kit for Drosophila melanogaster using P and piggyBac. Nat. Genet. *36*, 283–287.

Tran, T.S., Kolodkin, A.L., and Bharadwaj, R. (2007). Semaphorin regulation of cellular morphology. Annu. Rev. Cell Dev. Biol. *23*, 263–292.

Winberg, M.L., Mitchell, K.J., and Goodman, C.S. (1998a). Genetic analysis of the mechanisms controlling target selection: complementary and combinatorial functions of netrins, semaphorins, and IgCAMs. Cell *93*, 581–591.

Winberg, M.L., Noordermeer, J.N., Tamagnone, L., Comoglio, P.M., Spriggs, M.K., Tessier-Lavigne, M., and Goodman, C.S. (1998b). Plexin A is a neuronal semaphorin receptor that controls axon guidance. Cell *95*, 903–916.

Wu, Z., Sweeney, L.B., Ayoob, J.C., Chak, K., Andreone, B.J., Ohyama, T., Kerr, R., Luo, L., Zlatic, M., and Kolodkin, A.L. (2011). A combinatorial semaphorin code instructs the initial steps of sensory circuit assembly in the Drosophila CNS. Neuron *70*, 281–298.

Yu, H.H., Araj, H.H., Ralls, S.A., and Kolodkin, A.L. (1998). The transmembrane Semaphorin Sema I is required in Drosophila for embryonic motor and CNS axon guidance. Neuron *20*, 207–220.

Zhu, S., Lin, S., Kao, C.F., Awasaki, T., Chiang, A.S., and Lee, T. (2006). Gradients of the Drosophila Chinmo BTB-zinc finger protein govern neuronal temporal identity. Cell *127*, 409–422.